Journal of Nuclear Materials 467 (2015) 717–723

Contents lists available at ScienceDirect

Journal of Nuclear Materials

journal homepage: www.elsevier.com/locate/jnucmat

TEM examination of phases formed between U–Pu–Zr fuel and Fe

Assel Aitkaliyeva*, James W. Madden, Brandon D. Miller, Cynthia A. Papesch, James I. Cole

Idaho National Laboratory, Idaho Falls, ID 83415, USA

ARTICLE INFO

Article history:
Received 12 August 2015
Received in revised form
12 October 2015
Accepted 24 October 2015
Available online 28 October 2015

Keywords:
Metal fuel
U–Pu–Zr
Fuel-cladding chemical interaction (FCCI)

ABSTRACT

Exposure to high temperatures and irradiation results in interaction and interdiffusion between fuel and cladding constituents that can lead to formation of undesirable brittle or low-melting point phases. A diffusion couple study has been conducted to understand fuel-cladding interaction occurring between U–22Pu–4Zr (in wt%) fuel and pure Fe at elevated temperatures. The phases formed within fuel cladding chemical interaction (FCCI) layer have been characterized in the transmission electron microscope (TEM). The phases formed within FCCI layer have been identified as Fe_2U (Fd-3m), FeU_6 (I4/mcm), Fe_2Zr (Fd-3m), $FeZr_2$ (I4/mcm), Fe_2Pu (Fd-3m), UZr_2 (P6/mmm), β-Zr (Im-3m), and ZrO_2 (Fm-3m).

Published by Elsevier B.V.

1. Introduction

High burn-up, high fissile, inherent safety characteristics, favorable thermal response, and fertile density capability of the metallic fuels make them excellent candidates for next generation fast reactor applications [1,2]. Metallic fuels have disadvantages as compared to alternative fast reactor fuels (mainly ceramic based fuels), such as a propensity for developing fuel-cladding chemical interaction (FCCI) layers. Exposure to radiation in the nuclear reactor environment leads to swelling of the fuels and can result in intermixing and the formation of stable and metastable phases and precipitates. Contact between fuel matrix fission products and cladding promotes chemical and mechanical interactions, which can compromise integrity of the fuel and cladding.

Understanding interdiffusion phenomena is important for evaluation of the useful lifetime of nuclear reactor components and fuels. One of the important aspects is determining measurable materials changes associated with degradation in service that are indicative of incipient failure. For example, fast reactor fuels are often limited in operating characteristics or lifetime by interaction of the fuel or fission products with the fuel cladding materials. Detailed models for some of these effects, such as the fuel-cladding interactions, are just now being considered and data is needed to validate the models.

Phase relations in the quaternary iron–uranium–plutonium–zirconium (Fe–U–Pu–Zr) alloys have been previously investigated using thermal analysis techniques and energy dispersive spectroscopy (EDS) in the scanning electron microscope (SEM) [3]. In addition, out-of-pile annealing tests on diffusion couples have been conducted to investigate FCCI behavior between U–Zr and U–Pu–Zr fuel alloys and Fe, Fe–12Cr, and HT-9 cladding [4-8]. However, developing a detailed quantitative nano- and atomic-scale understanding of the microstructure and phases formed in quaternary Fe–U–Pu–Zr systems has not been achieved to date. Most of the previous work has been done using surface-based techniques, such as glancing angle X-ray diffraction (XRD) and SEM, which don't allow analysis of subsurface features and prevent conducting accurate analysis of Pu-based phases. Previously, preparation of transuranic fuels for transmission electron microscopy (TEM) has been associated with a large number of challenges and deemed impossible. Recent utilization of focused ion beam (FIB) instruments in the fields of nuclear fuels and materials have helped to overcome these issues.

In this study phases formed in a diffusion couple prepared from a U–22Pu–4Zr fuel and Fe have been examined in the TEM. Detailed structural and chemical composition analysis of the FCCI layer has been conducted. Selected-area electron diffraction (SAED) using transmission electron microscopy provides important space-group and lattice parameter information on the phases formed in this quaternary Fe–U–Pu–Zr system.

2. Materials and methods

A fuel alloy with nominal composition of U–22Pu–4Zr (in wt%) and Fe (99.995% purity, obtained from Alfa Aesar, Ward Hill, MA)

* Corresponding author.
E-mail addresses: assel.aitkaliyeva@inl.gov, assel.aitkaliyeva@gmail.com (A. Aitkaliyeva).

http://dx.doi.org/10.1016/j.jnucmat.2015.10.043
0022-3115/Published by Elsevier B.V.

cladding were selected for this diffusion couple study. The fuel was arc cast in an inert atmosphere glove box using a drop casting technique. The produced cylindrical fuel slugs were sectioned into several pieces designated for assembling a diffusion couple. The surfaces of both fuel and cladding sections were polished through a 3 μm diamond solution. The polished fuel and the cladding surfaces were placed in contact and compressed to 6 in-lbs. in a Kovar steel jig, lined with tantalum foil on the interior to prevent an undesirable reaction between diffusion couples and the jig.

It is possible that oxides formed on the surface of the fuel and the initial fuel-cladding interface, as even ultra-high purity argon can contain oxygen and other reacting gases. Therefore, some of the phases formed upon heat treatment could have been stabilized by impurities. The diffusion couple was annealed at 700 °C for 75 h in a furnace under continuous argon flow (Ar purity of 99.999%, the flow rate has not been measured). Immediately after annealing, the assembly was quenched in water to preserve the phases formed upon heat treatment. The diffusion couple was removed from the compression device and mounted with the fuel cladding interface perpendicular to the analysis surface in epoxy. The surface of the diffusion couple was polished through a 1 μm diamond solution prior to analysis.

The surface of the diffusion couple was initially examined in FEI QUANTA 3D field emission gun (FEG) dual beam focused ion beam/scanning electron microscope (FIB/SEM), operated at electron accelerating voltage of 20 kV during examination. The exact location of the fuel-cladding interaction zone was determined and an examination of the formed microstructure was conducted. Upon completion of initial examination, seven cross-sectional specimens for transmission electron microscopy (TEM) were prepared. TEM specimens were characterized at 200 kV in a JEOL JEM 2010 TEM equipped with Bruker Quantax 200 Esprit 1.9 software and a Bruker 133 silicon drift detector.

Seven cross-sectional specimens were prepared from the FCCI region, shown in Fig. 2, and characterized in TEM. Multiple lift-outs were prepared to ensure thorough characterization and identification of all phases. The lamella had approximate dimensions of 20 μm × 10 μm × 0.1 μm. Identification of formed phases was conducted by comparing experimental selective area electron diffraction (SAED) patterns to simulated patterns from published crystal structures produced using JEMS software [9]. In addition, d spacing of each diffraction pattern was measured and compared to the published crystallographic data. The data from four cross-sectional lift-outs is provided in this work since the phases present in the other lift-outs were consistent with data shown here.

Multiple cross-sectional TEM specimens containing U–Pu enriched matrix have been prepared in the FIB tool but due to differential thinning of diverse phase constituents in these multi-component diffusion couples, most U–Pu enriched phases were not sufficiently thin to acquire SAD patterns. Since both U and Pu have larger atomic masses as compared to other elements in these samples, U–Pu enriched phases thin at a much slower rate. In addition, Pu-enriched phases oxidized more rapidly during specimen transfer between instruments than other phases within prepared lamella. Because of these issues, identification of U–Pu enriched phases in TEM has not been conducted. Further investigation into sample preparation will be conducted to overcome these issues.

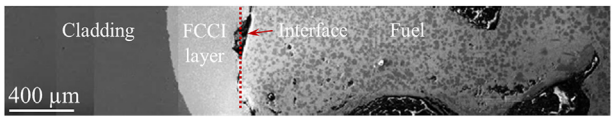

Fig. 1. Overview of the cladding, formed fuel-cladding interaction layer, and fuel after annealing. The red dot line shows the position of the initial fuel-cladding interface. The scale bar denotes 400 μm. (For interpretation of the references to color in this figure legend, the reader is referred to the web version of this article.)

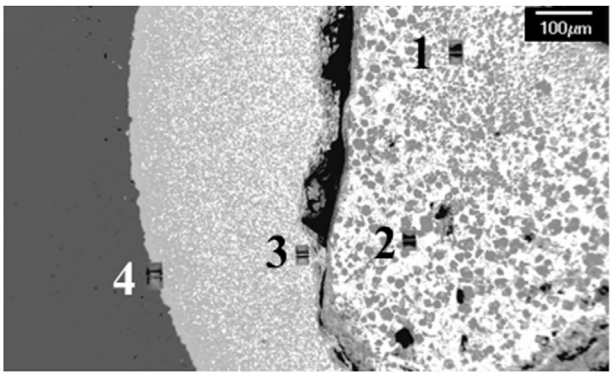

Fig. 2. Backscattering electron micrograph depicting positions of the lift-outs within FCCI layer. The numbers identify the lift-out location.

3. Results and discussion

In this work the phases formed in the quaternary U–Pu–Zr–Fe system have been investigated using diffusion couple technique. At the early stages of diffusion Fick's law governs atom penetration. When the thermal budget is sufficiently high, the concentration profile evolves into step height distributions, with each step corresponding to an equilibrium phase predicted by the phase diagram. A diffusion couple can be formed at a pre-selected temperature and is quickly quenched into to ambient temperature. Thus, the microstructure corresponding to a higher temperature in the phase diagram is retained to a low temperature for characterization, and temperate dependences of phase diagrams can be systematically studied in this way.

Fig. 1 shows the secondary electron micrograph depicting Fe, fuel, and formed fuel-cladding interaction layer. The acquired micrographs and X-ray maps revealed substantial diffusion of the fuel into the cladding, with a width of the FCCI layer at about 425 ± 85 μm. As it can be seen, the formed FCCI layer was not uniform in width, with some areas having smaller FCCI width. Different contrast seen in the micrograph is an artifact of multiple image acquisitions followed by stitching of the micrographs. The positions of four lift-outs of interest are provided in Fig. 2.

Fig. 3 shows elemental X-ray maps and the corresponding scanning transmission electron micrographs collected from the first lift-out. EDS point scans were collected but not quantified due to unavailability of standards for transuranic elements. X-ray maps depicting spatial distributions of various elements were collected by individually mapping characteristic X-rays from each element of interest with the EDS spectrometer in TEM. Each map was adjusted for contrast and brightness to emphasize spatial variations in intensity. Brighter areas in each map represent higher concentrations of the element of interest than less bright areas in the same map. Note that equally bright areas in different maps do not represent comparable concentrations. Elemental X-ray maps shown in Fig. 3 revealed segregation of U and Pu in the matrix, Fe and U/Pu, and Fe with Zr. This suggests formation of three distinctive phases within the first lift-out.

Assessment of ternary Fe–U–Pu, Fe–U–Zr, and Pu–U–Zr systems conducted by other research groups allowed constructing an isothermal section for quaternary U–Pu–Zr–Fe system shown in Fig. 4 [3,6–8,10]. An isothermal section of the Fe–U–Pu system at

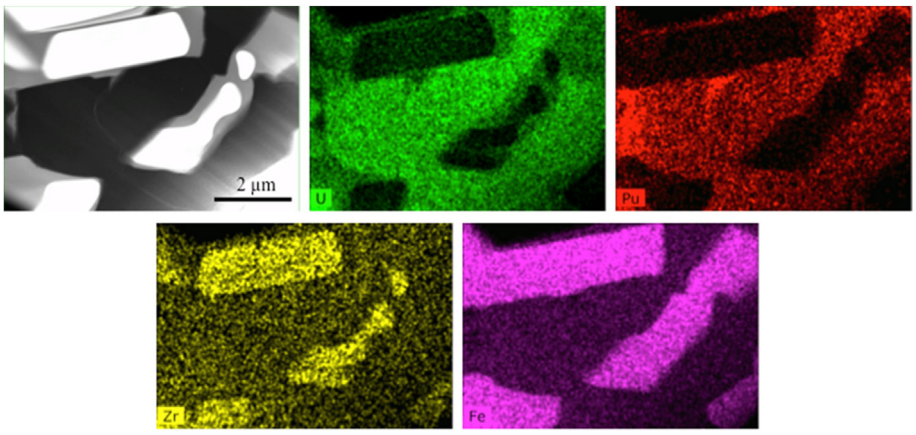

Fig. 3. Scanning transmission electron micrograph and corresponding X-ray maps of the phases formed between U–22Pu–4Zr fuel and Fe cladding upon heat treatment at 700 °C. Scale bar denotes 2 μm. The maps were acquired from the first lift-out.

700 °C shows formation of FeU_6, Fe_2U, Fe_2Pu, β-U, η, α-Fe, and bcc phase, also known as (U, Pu)ht. The Fe_2Pu phase has three polymorphic forms: cubic Laves phase of the C15-type, hexagonal Laves phase of the $MgNi_2$-type, and cubic phase that is stable above 1040 °C. The Laves phase Fe_2U has the C15-type cubic structure, and FeU_6 has the MnU_6-type tetragonal structure. In the Fe–U–Zr system, the following phases can form at 700 °C: α-Fe, α-U, α-Zr, Fe_2Zr, $FeZr_2$, $Fe_{23}Zr_6$, $FeZr_3$, Fe_2U, FeU_6, χ, ε, and λ. The Fe_2Zr phase can exist in cubic C15-type and hexagonal C36-type forms. The tetragonal $FeZr_2$ phase has a narrow temperature range of 951–780 °C and orthorhombic $FeZr_3$ phase occurs below 851 °C. The cubic $Fe_{23}Zr_6$ phase is not in equilibrium as it is stabilized by oxygen.

Evaluation of Pu–U–Zr subsystem confirms the presence of (U, Pu)ht (known as γ-U), α-Zr, α-U, β-U, η, and ζ phases. The hexagonal δ-UZr_2 phase has an AlB_2 type structure, is non-stoichiometric, and should have extensive solid solubility for plutonium. The ζ-(U, Pu) phase belongs to the *R-3m* space group with 58 atoms in the primitive unit cell and ten atoms in the asymmetric unit. The ζ is stabilized by the presence of Zr. Previously conducted experimental studies report formation of Fe_2Zr, Fe_2U, $Fe(Pu, U)_6$, λ phase ($Fe_{0.06}U_{0.69\text{-}0.73}Zr_{0.21\text{-}0.25}$) χ phase ($Fe_{0.5}U_{0.18}Zr_{0.32}$), ε phase ($Fe_{0.33}U_{0.17\text{-}0.34}Zr_{0.33\text{-}0.5}$), and solid solution consisting of γ-U, ε-Pu, and β-Zr in quaternary U–Pu–Zr–Fe system [3]. However, since these results were based on X-ray results only, no crystallographic information has been reported.

Based on the segregation of the elements in X-ray maps shown in Fig. 3, initial phase identification was conducted by consulting the phase diagram provided in Fig. 4. The Fe–Zr enriched phases could correspond to one of the indicated Fe–Zr stoichiometric phases. The Fe–U enriched region could be either Fe_2U or FeU_6. However, due to overlap of U and Pu peaks, this region could correspond to Fe_2Pu or $FePu_6$. The matrix can correspond to (U, Pu) ht, ζ-(U, Pu), α-U, or β-U. Selective area electron diffraction patterns of the phases similar to those shown in Fig. 3 were collected, analyzed, and provided in Fig. 5. The numbers provided in the micrograph indicate location of different phases. The Fe–Zr enriched phase was identified as Fe_2Zr and Fe–U/Pu enriched phase corresponds to Fe_2Pu. The Fe_2Zr phase is surrounded by Fe_2Pu, which was been observed in several lift-outs. Due to the varying FIB milling rates and subsequent specimen thickness variation, the U–Pu enriched matrix was not sufficiently thin for SAD analysis and therefore identification of the U–Pu enriched phase has not been conducted.

Fig. 6 shows bright-field (BF) transmission electron micrograph of the phases formed at the top of the first lift-out and experimental SAED patterns corresponding to the phases identified in the lift-out. Numbers provided in the micrograph indicate location of different phases, which were identified as $FeZr_2$ and Fe_2U. Simulated electron diffraction patterns are provided on the

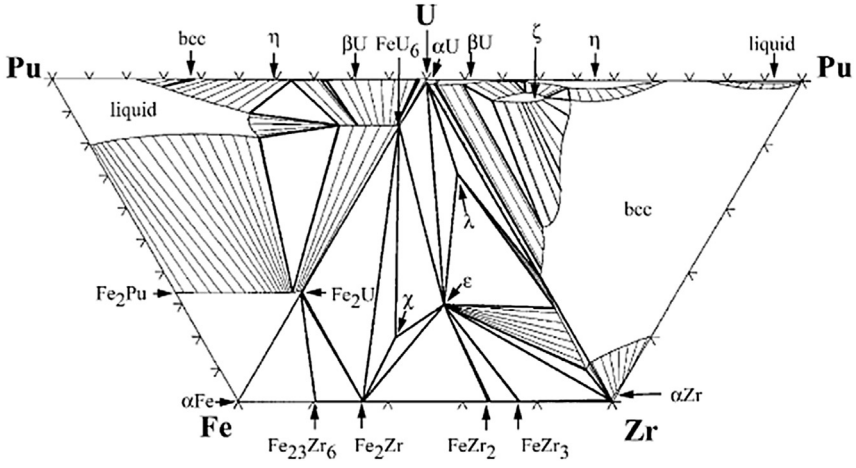

Fig. 4. Assessed isotherms for the ternary Fe–U–Pu, Fe–U–Zr, and Pu–U–Zr systems at 700 °C. Reprinted from Ref. [3].

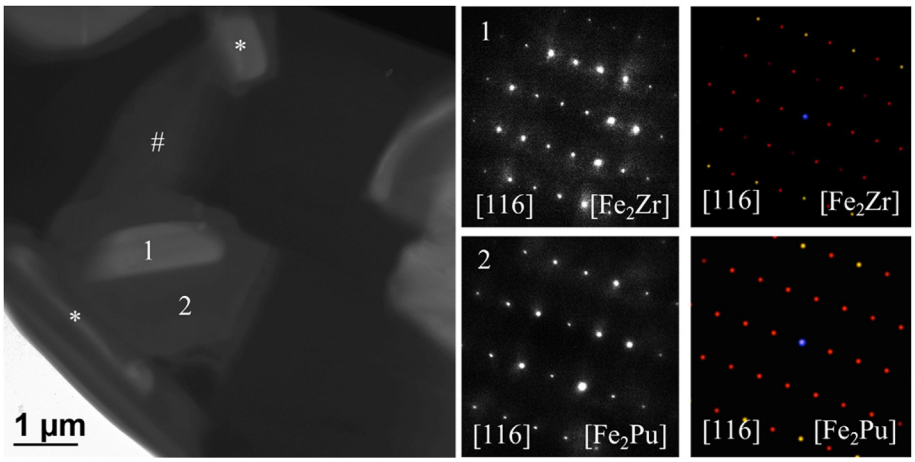

Fig. 5. Transmission electron micrograph acquired from the first lift-out within FCCI layer and corresponding experimental (middle row) and simulated (right row) SAED patterns. Scale bar denotes 1 μm. The asterisk denotes location of other Fe_2Zr phases and the # denotes location of Fe_2Pu phases.

right side of Fig. 5 for reference. The $FeZr_2$ and Fe_2U behavior resembles that of Fe_2Zr and Fe_2Pu, where $FeZr_2$ is surrounded by Fe_2U phase. The phase with the lightest contrast in Fig. 6 corresponds to $FeZr_2$ and the darker phase is consistent with Fe_2U. The Fe_2U phase formed in the immediate vicinity of $FeZr_2$ phase in multiple lift-outs.

Fig. 7 shows elemental X-ray maps and corresponding scanning transmission electron micrograph collected from another region within the first lift-out. The elemental constituents can be classified into several groups in which they exhibit similar behavior and segregate into common phases. Qualitative examination of STEM micrograph and X-ray maps shown in Fig. 7 suggests segregation of Zr in the bright contrast areas, U with Zr, Fe with Zr, Fe with U, and U with Pu in the matrix.

The U–Zr enriched phases were identified as δ-UZr_2 and Zr enriched phases were identified as ZrO_2. Indexed experimental SAD patterns of phases identified in the second lift-out and simulated electron diffraction patterns are provided in Fig. 8. The ZrO_2 precipitates are encapsulated by δ-UZr_2 phase, as it can be seen in the bright field TEM micrographs (Fig. 8). The light contrast Fe–Zr enriched phase in the top right corner of the figure has been identified as $FeZr_2$ and darker contrast Fe–U enriched band around it has been identified as Fe_2U. The diffraction patterns corresponding to these two phases are not provided as similar SAED patterns have been provided in Fig. 6.

Bright-field transmission electron micrograph and corresponding SAED patterns from a second lift out provided in Fig. 9 show a behavior different from the behavior observed in the first lift-out. Here the Fe_2Zr phase forms in the immediate vicinity of the FeU_6 phase, and not Fe_2Pu phase. Numbers provided in the micrograph indicate location of Fe_2Zr and FeU_6 phases, and symbols identify location of other regions consistent with these phases.

Fig. 10 shows bright-field transmission electron micrograph of the Zr precipitate observed in the third lift-out and its corresponding experimental and simulated electron diffraction patterns. Formation of high-Zr inclusions has been previously reported in a variety of transmutation fuels [11–18]. These precipitates were assumed to be α-Zr stabilized by dissolved impurities such as N, O, C, Cl, C, and Si. However, existing actinide-Zr phase diagrams indicate that α-Zr, which is considered to be the equilibrium room-temperature Zr phase, should not form. Previously published reports were predominantly based on micro-chemical analyses of individual precipitates without crystal-structure information and X-ray diffraction information without chemical data. Therefore, such reports assumed that Zr inclusions correspond to impurity-stabilized α-Zr. However, recent TEM work conducted by Janney

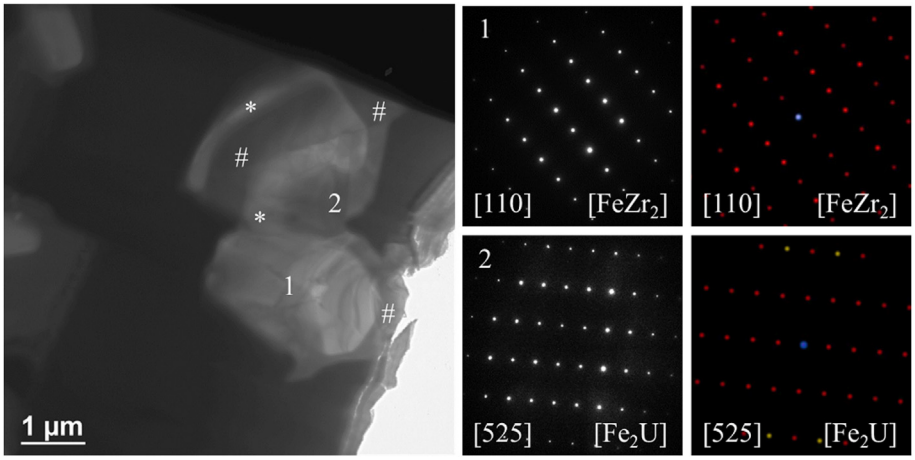

Fig. 6. Transmission electron micrograph acquired from the first lift-out within FCCI layer and corresponding experimental (middle row) and simulated (right row) SAED patterns. Scale bar denotes 1 μm. The asterisk denotes location of other $FeZr_2$ phases and the # denotes location of Fe_2U phases.

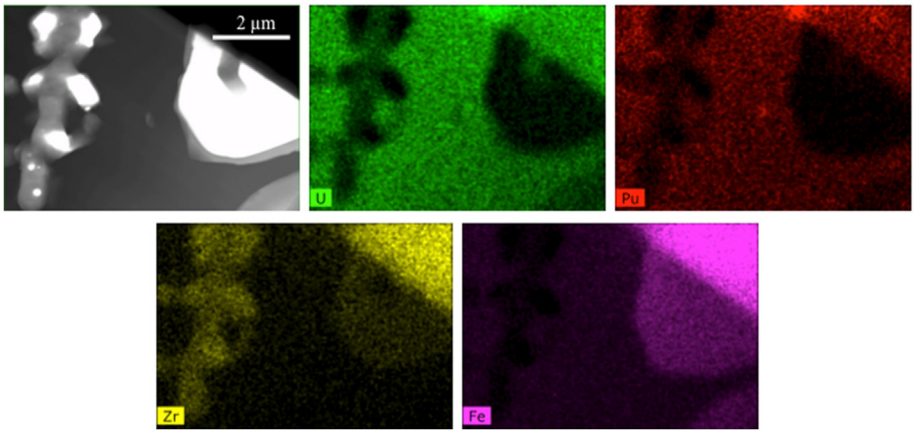

Fig. 7. Scanning transmission electron micrograph and corresponding X-ray maps of the phases formed in the first lift-out. Scale bar denotes 2 μm.

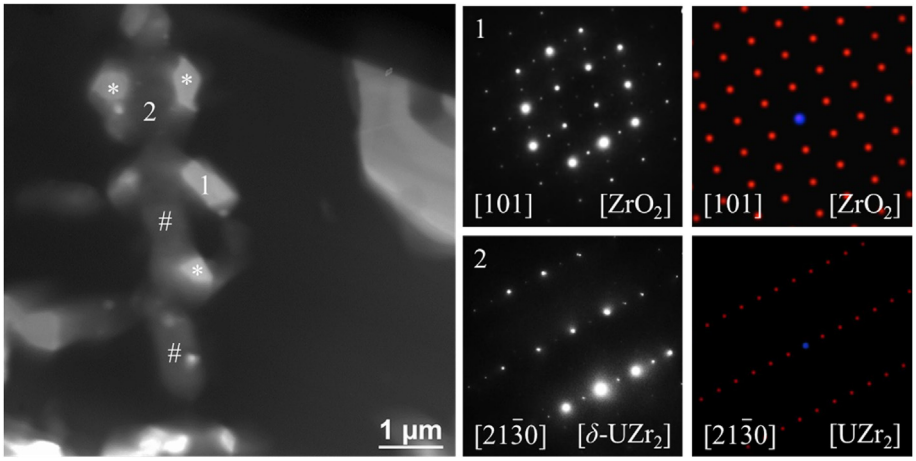

Fig. 8. Transmission electron micrograph acquired from the first lift-out and corresponding experimental (middle row) and simulated (right row) SAED patterns. Scale bar denotes 1 μm. The asterisk denotes location of other ZrO_2 phases and the # identifies additional UZr_2 phases present in the micrograph.

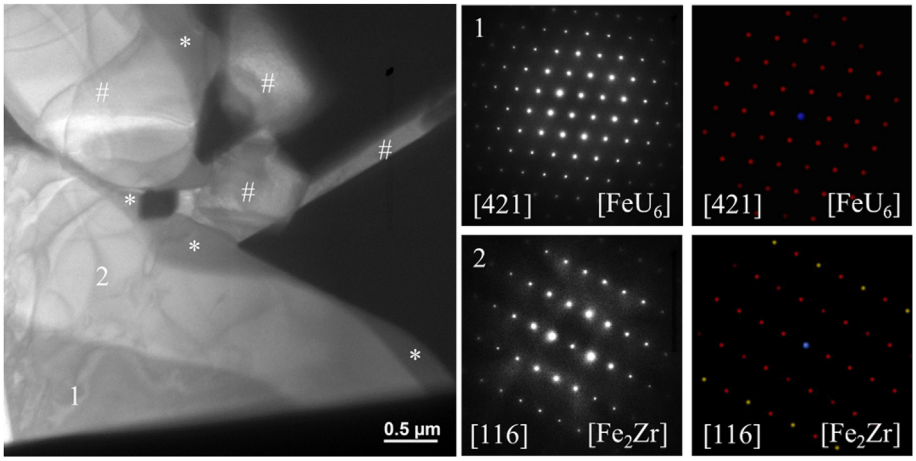

Fig. 9. Transmission electron micrograph acquired from the second lift-out within FCCI layer and corresponding experimental (middle row) and simulated (right row) SAED patterns. Scale bar denotes 0.5 μm. The asterisk denotes location of other FeU_6 phases and the # denotes location of Fe_2Zr phases.

et al. showed that even though chemical compositions of high-Zr inclusions are consistent with previous reports, the crystal structure of precipitates is face-centered cubic [16]. Previous work on U–25Pu–14Zr (wt%) fuel showed formation of β-Zr precipitates as well [18]. Formation of fcc Zr inclusion has been reported in nanocrystals and thin films but not in larger crystals [19–20]. It is possible that impurities such as N are responsible for the observed β-Zr as the impurities most likely acted as a stabilizing element.

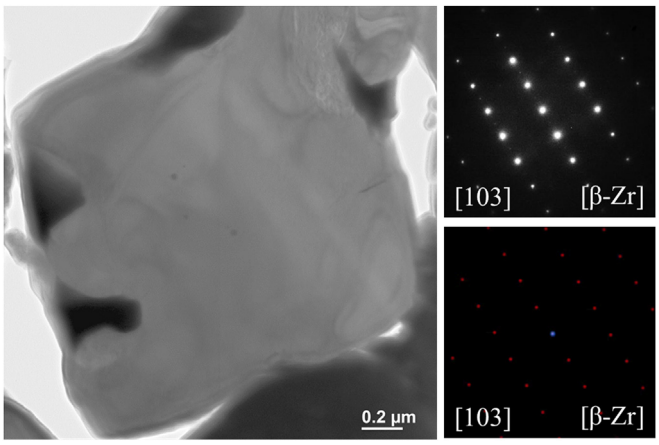

Fig. 10. Transmission electron micrograph acquired from the third lift-out and corresponding experimental (top row) and simulated (bottom row) SAED patterns of β-Zr. The scale bar denotes 0.2 μm.

Fig. 11 shows bright-field transmission electron micrograph overview of the phases observed in the TEM specimens lifted-out from the end of the FCCI layer. Numbers provided in the figure indicate location of Fe_2U phase, formed at the end of the diffusion zone, and Fe. Experimental and simulated electron diffraction patterns are provided on the right side of Fig. 11 for reference. The summary of all phases observed within FCCI region is provided in Table 1.

Previous reports identify formation of the Fe_2Zr, Fe_2U, $Fe(Pu,U)_6$, a solid solution of $\gamma U + \beta Pu + \beta Zr$, λ phase ($Fe_{0.06}U_{0.69\text{-}0.73}Zr_{0.21\text{-}0.25}$) χ phase ($Fe_{0.5}U_{0.18}Zr_{0.32}$), and ε phase ($Fe_{0.33}U_{0.17\text{-}0.34}Zr_{0.33\text{-}0.5}$) in quaternary U–Pu–Zr–Fe alloy [3]. However, most of previously published research relied on micro-chemical analysis of phases without crystal-structure determination or X-ray diffraction data without chemical analysis of individual phases. Both of these techniques are surface based and do not permit identification of the phases that form beneath specimen surface. We have previously shown that surface oxidation can prevent accurate phase identification in these U–Pu–Zr alloys [17]. Therefore, it is imperative to examine phases formed beneath specimen surface and provide crystallographic information on the phases formed within the FCCI layer. Cross-sectional TEM specimens prepared in the FIB show the microstructure of the fuel beyond the surface layer. Hence, the observed discrepancy between this work and the previously conducted research is not surprising.

The present study suggests the clear need to identify phases in transuranic fuels using a combination of techniques and not to rely on micro-chemical analysis or XRD data only. A number of subsurface features identified within the FCCI layer prove that detailed analysis is needed to fully understand formation of phases and the complex FCCI phenomena. Caution should also be taken during identification of Zr-enriched inclusions in U–Pu–Zr fuels. As it has been shown in this work, not all Zr precipitates are consistent with α-Zr. Many factors can affect which Zr crystal structure is formed in the specimen, such as compositions, casting techniques, and heat treatment histories.

4. Summary

The present research used SAED pattern analysis in transmission electron microscope to identify the phases formed between U–22Pu–4Zr and Fe cladding. Substantial fuel-cladding chemical interaction layer has been observed upon heat treatment of the diffusion couple at 700 °C. The thickness of the FCCI layer was not uniform with the average thickness in the order of 425 ± 85 μm. The phases formed within the FCCI layer were identified as: Fe_2U, FeU_6, Fe_2Zr, $FeZr_2$, Fe_2Pu, δ-UZr_2, β-Zr, and ZrO_2. The cladding was consistent with α-Fe. Examination of multiple lift-outs revealed formation of the Fe_2Zr in the immediate vicinity of Fe_2Pu and FeU_6 phases. The $FeZr_2$, on the other hands, tends to form next to Fe_2U phase, and in most cases Fe_2U encapsulates $FeZr_2$ phase. Similar behavior has been observed between ZrO_2 and δ-UZr_2 phases, where the δ-UZr_2 phase surrounds ZrO_2 precipitates. Formation of β-Zr inclusions has been noted in this work. The presence of impurities such as N can be responsible for Zr stabilization in the face-centered cubic form. The Pu–U enriched matrix phase has not been identified using SAED analysis due to differential thinning of diverse phase constituents in FIB tool. However, in accordance with existing phase diagrams, these phases could correspond to either βU, (εPu,γU), or ($\varepsilon + L$).

U.S. Department of Energy Disclaimer

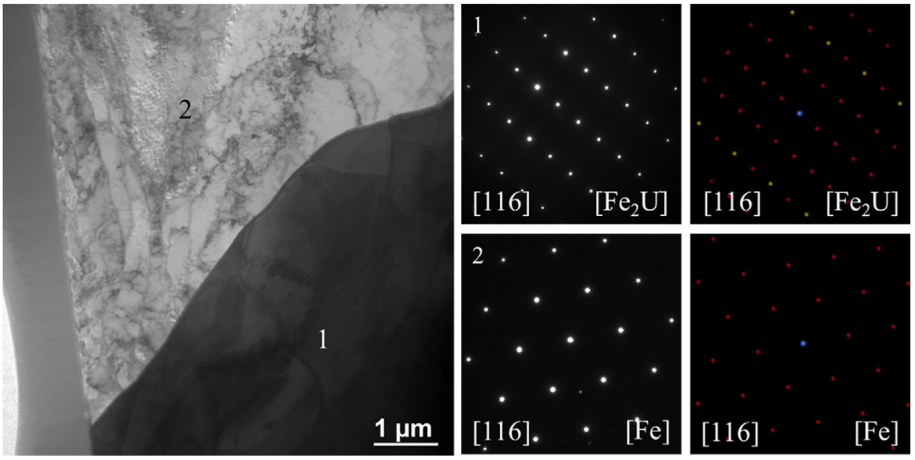

Fig. 11. Transmission electron micrograph acquired from the fourth lift-out prepared from the end of FCCI region and corresponding experimental (middle row) and simulated (right row) SAED patterns. Scale bar denotes 1 μm.

Table 1
Summary of the phases observed within the FCCI layer.

Phase	Space group	Unit cell parameters, nm	Lift-out location
Fe_2U	Fd-3m O2 (227)	a = 0.7057	1, 4
FeU_6	I4/mcm (140)	a = b = 1.0303; c = 0.5235	2
Fe_2Zr	Fd-3m O2 (227)	a = 0.7075	1, 2
$FeZr_2$	I4/mcm (140)	a = b = 0.6409; c = 0.5593	1
Fe_2Pu	Fd-3m O2 (227)	a = 0.7183	1
δ-UZr_2	P6/mmm (191)	a = b = 0.503; c = 0.308	1
β-Zr	Im-3m (229)	a = 0.3551	3
ZrO_2	Fm-3m (225)	a = 0.5118	1

Acknowledgments

This work is supported by the U.S. Department of Energy, under DOE Idaho Operations Office Contract DE-AC07-05ID14517, as part of Fuel Cycle Research and Development (FCRD) program of US Department of Energy and Nuclear Science User Facilities (NSUF).

References

[1] D.E. Burkes, R.E. Fielding, D.L. Porter, J. Nucl. Mater. 392 (2009) 158.
[2] Y.S. Kim, G.L. Hofman, S.L. Hayes, Y.H. Sohn, J. Nucl. Mater. 327 (2004) 27.
[3] K. Nakamura, T. Ogata, M. Kurata, T. Yokoo, M.A. Mignanelli, J. Nucl. Mater. 304 (2002) 63.
[4] D.D. Keiser Jr., M.C. Petri, J. Nucl. Mater. 240 (1996) 51.
[5] D.D. Keiser Jr., M.A. Dayananda, J. Nucl. Mater. 200 (1993) 229.
[6] K. Nakamura, T. Ogata, M. Kurata, A. Itoh, M. Akabori, J. Nucl. Mater. 275 (1999) 246.
[7] T. Ogata, M. Kurata, K. Nakamura, A. Itoh, M. Akabori, J. Nucl. Mater. 250 (1997) 171.
[8] A.B. Cohen, H. Tsai, L.A. Neimark, J. Nucl. Mater. 204 (1993) 244.
[9] P. Stadelmann, JEMS (EMS Java Version), CIME-EPFL, Lausanne, Switzerland, 2004.
[10] V. Raghavan, J. Phase Equilibria 24 (2003) 367.
[11] Y.H. Sohn, M.A. Dayananda, G.L. Hofman, R.V. Strain, S.L. Hayes, J. Nucl. Mater. 279 (2000) 317.
[12] R.D. Mariani, et al., Phase Studies and Property Measurements of Some Ternary Fuel Alloys, AFC2-B General Fuel Characterization Report, INL/EXT-09–16781, Idaho National Laboratory, 2009.
[13] D.R. O'Boyle, A.E. Dwight, Uranium-plutonium-zirconium ternary alloy system, in: Proc., 4th International Conference on Plutonium and Other Actinides, 1970, pp. 720–732.
[14] L. Leibowitz, et al., J. Nucl. Mater. 154 (1998) 145.
[15] C.L. Trybus, J.E. Sanecki, S.P. Henslee, J. Nucl. Mater. 204 (1993) 50.
[16] D.E. Janney, J.R. Kennedy, J.W. Madden, T.P. O'Holleran, J. Nucl. Mater. 448 (2014) 109.
[17] A. Aitkaliyeva, J.W. Madden, C.A. Papesch, J.I. Cole, TEM identification of subsurface phases in ternary U-Pu-Zr fuel, J. Nucl. Mater. (2015) (submitted for publication).
[18] A. Aitkaliyeva, J.W. Madden, B.D. Miller, C.A. Papesch, J.I. Cole, Fuel-cladding interaction between U-Pu-Zr fuel and Fe, Metall. Mater. Trans. E (2015) (in press).
[19] I. Manna, P.P. Chattopadhyay, F. Banhart, H.-J. Fecht, Appl. Phys. Lett. 81 (2002) 4136.
[20] E.B. Dolgusheva, V.Y. Trubitsyn, Phys. Solid. State 54 (2012) 1552.